New predictive model for monitoring bone remodeling

Habiba Bougherara,[1] Václav Klika,[2,3] František Maršík,[3] Ivo A. Mařík,[4] L'Hocine Yahia[5]
[1]*Department of Mechanical and Industrial Engineering, Ryerson University, Toronto, Canada M5B 2K3*
[2]*Department of Mathematics, FNSPE, Czech Technical University in Prague, Trojanova 13, 120 00, Prague 2, Czech Republic*
[3]*Institute of Thermomechanics, Czech Academy of Sciences, Dolejskova 5, 18200 Prague 8, Czech Republic*
[4]*Department of Anthropology and Human Genetics, Ambulant Centre for Defects of Locomotor Apparatus, Faculty of Sciences, Charles University Prague, Olšanská 7, CZ-130 00 Prague 3, Czech Republic*
[5]*Laboratory for Innovation and Analysis of Bioperformance (LIAB), École Polytechnique, Montréal, Québec, Canada H3T 1J4*

Received 18 May 2008; revised 13 February 2009; accepted 22 September 2009
Published online 10 June 2010 in Wiley Online Library (wileyonlinelibrary.com). DOI: 10.1002/jbm.a.32679

Abstract: The aim of this article was to present a new thermodynamic-based model for bone remodeling which is able to predict the functional adaptation of bone in response to changes in both mechanical and biochemical environments. The model was based on chemical kinetics and irreversible thermodynamic principles, in which bone is considered as a self-organizing system that exchanges matter, energy and entropy with its surroundings. The governing equations of the mathematical model have been numerically solved using Matlab software and implemented in ANSYS software using the Finite Element Method. With the aid of this model, the whole inner structure of bone was elucidated. The current model suggested that bone remodeling was a dynamic process which was driven by mechanical loading, metabolic factors and other external contributions. The model clearly indicated that in the absence of mechanical stimulus, the bone was not completely resorbed and reaches a new steady state after about 50% of bone loss. This finding agreed with previous clinical studies. Furthermore, results of virtual computations of bone density in a composite femur showed the development of a dense cortical bone around the medullary canal and a dense trabeculæ bone between the femoral head and the calcar region of the medial cortex due to compressive stresses. The comparison of the predicted bone density with the structure of the proximal femur obtained from X-rays and using strain energy density gave credibility to the current model. © 2010 Wiley Periodicals, Inc. J Biomed Mater Res 95A: 9–24, 2010

Key words: bone remodeling; open system thermodynamics; bone biochemistry; dynamical loading; metabolic factors

INTRODUCTION

The clinical outcome of orthopedic implant procedures relies on many factors, but there is general agreement that two issues are of paramount importance. The first is the mechanical stability, which depends on implant migration, and shedding particulate matter from the implant surface.[1] The second is the pattern of bone ingrowth and adaptive bone remodeling (stress shielding) resulting from the complex interaction of strain patterns, implant material and structural properties and bone characteristics.[2] Bone remodeling is of considerable concern because it can result in a significant amount of bone resorption in the vicinity of the implant.[3] Bone remodeling thus requires attention in the follow-up of clinical cases and in the design process of new prostheses.

Several mathematical models have been proposed to explain the relationship between mechanical forces and bone structure. These models can be classified into three groups: Mechanical, mechanobiological, and biochemical.[4–13]

Mechanical theories of bone adaptation have been previously developed to predict changes in bone shape- and density-based different kind of mechanical stimuli, e.g., stress, strain, strain energy density, mechanical damage.[4,7,14,15] These models are based on Wolff's Law (i.e., "use it or lose it") and generally yield a time rate of change of bone density to a mechanical stimulus. These continuum models have achieved some success in predicting normal bone

Correspondence to: H. Bougherara; e-mail: habiba.bougherara@ryerson.ca

Contract grant sponsors: Ryerson University, NSERC Discovery Grant
Contract grant sponsor: Grant Agency of the Czech Republic (GACR); contract grant numbers: 106/03/1073, 106/03/0958

architecture. However, as Huiskes et al.[7] pointed out, they involve three major deficiencies. First, they use mechanical stress or strain to predict bone remodeling behavior, without considering biological mechanisms. Second, they consider bone as a continuum material, for which only the theories of linear elasticity are valid. Third, the theories behind these models are (quasi) static ones, thus effects of load rates and nonlinear (visco-elastic) properties are not included.

Mechanobiological models were initially introduced via Frosts' "mechanostat" theory.[16] This theory proposes that bone adapt its strength to keep the strain caused by physiological loads close to a set-point. If strain levels exceed a set-point, new bone is formed, and below this set-point, bone is removed. The mechanostat is a qualitative theory because the set-point is not specified; nevertheless, this theory was the basis for the development of several new mathematical and computational models to study bone adaptation.[10,13,17,18]

Biochemically, few models have been based on the activities of bone cells known as osteoclasts and osteoblasts have been developed to obtain insight into the bone remodeling process at the cellular level. The first of this kind of model described the differential activity of Parathyroid Hormone as a regulator for bone resorption and formation.[19,20] The second model demonstrated the critical role of hormones such as autocrine and paractine in the regulation of bone remodeling.[21] The third model proposed a signaling pathway known as RANK/RANKL/OPG (i.e., receptor activator of proteins and genes is known to play a key role in bone remodeling) to regulate bone cells activities.[12] While these cell-based models give insight into bone regulation mechanisms considering metabolic factors, none of them considered the mechanical stimulus which plays an important role in load-induced bone remodeling.[22] However, in order to improve the understanding of bone remodeling, it is crucial to include all factors (i.e., mechanical, biological, and biochemical) concurrently.

A relatively new model (a biochemomechanical model) for bone resorption which does not fall exclusively into each of the aforementioned categories was proposed by Rouhi et al.[11] This model is based on the mixture theory combined with chemical reactions. The model may be useful for modeling growth and adaptation of biological tissues.

To the authors' knowledge, however, no prior investigations have been based on nonequilibrium (or irreversible) thermodynamic principles, in which the bone is considered as a self-organizing system that exchanges matter, energy, and entropy with its surroundings. Thus, the use of irreversible thermodynamics to link the mechanical factors to the metabolic (chemical and biological) ones has not been assessed. This may increase the potential of the model to investigate bone resorption related diseases such as osteoporosis and provide more insight into stem cell therapy, by controlling the process of bone remodeling. This can be achieved by integrating the bone growth control pathways such as RANK-RANKL-OPG pathway.[23] Virtually, bone tissue can be amenable to cellular therapy and only preclinical models and subsequent clinical treatment can identify the susceptibility of a given disease to such therapy. The current model is a starting point to reach this goal.

The purpose of this study was to introduce a new thermodynamic-based framework for bone remodeling. It was hypothesized that the dynamic loading is linked to metabolic biological and chemical factors. Outcome simulations included time evolution of bone concentration and effects of mechanical and metabolic parameters. The results were compared with clinical data and a finite element model using strain energy density developed previously by some of the authors to investigate bone remodeling in a new biomimetic composite hip stem.[24]

MATERIALS AND METHODS

Biochemical description of bone remodeling process

Bone remodeling is a complex process performed by the coordinated activities of bone cells known as osteoblasts and osteoclasts. This process can be divided into three stages: bone resorption, formation, and growth control. In the proposed model, the authors focused on bone resorption and formation.

The governing chemical reactions for both bone resorption and formation were formulated based on the existing knowledge of bone cell regulation and interaction.[25] The developed chemical reactions (ρ = 1–5) were amended based on the assumption that, in nature, structures are well optimized (i.e., "little waste").[26] In other words, products resulting from bone decomposition (D_7) participated in formation of new bone. All considered chemical reactions describing the mechanism of bone remodeling (ρ = 1–5) had the general form of Menten-Michaelis enzyme reaction[27,28] (see Appendix A), i.e.,

$$[\text{Substrate}] \underset{k_-}{\overset{k_+}{\rightleftarrows}} [\text{Product}]$$

The only cells that are able to resorb bone tissue are osteoclasts. To be active, they need to be coupled in multinucleated complex, whose formation can be described as follows:

$$D_1 + \text{MCELL} \underset{k_{-1}}{\overset{k_{+1}}{\rightleftarrows}} \text{MNOC} + D_4 \qquad (\rho = 1)$$

where D_1 is mixture of substances that are initiating the reaction with mononuclear cells (MCELL). MNOC refers to multinucleated osteoclasts and D_4 is a remaining product from the ρth reaction.

The osteoclast cells break down bone by acting on bone to erode minerals and the matrix. This action was described by the following reaction:

$$\mathrm{MNOC} + \mathrm{Old\_B} \underset{k_{-2}}{\overset{k_{+2}}{\rightleftarrows}} D_6 + D_7 \qquad (\rho = 2)$$

where Old_B is the abbreviation for old bone, and D_6 and D_7 are products made during bone decomposition. Because biological processes are well optimized, a part of the product D_7 participated in the activation of osteoblasts.

Before osteoblasts (OB) repair and fill the eroded cavities, they need to be activated by the activator (Activ_OB), which is produced after bone resorption. The action of osteoblasts was described as follows

$$D_7 + \mathrm{Old\_B} \underset{k_{-3}}{\overset{k_{+3}}{\rightleftarrows}} \mathrm{Activ\_OB} + D_9 \qquad (\rho = 3)$$

$$\mathrm{Activ\_OB} + \mathrm{OB} \underset{k_{-4}}{\overset{k_{+4}}{\rightleftarrows}} \mathrm{Osteoid} + D_{12} \qquad (\rho = 4)$$

where D_{12} is a remaining substratum.

The final stage of remodeling was bone calcification. The bone surface is restored and covered by a layer of lining cells according to:

$$D_{13} + \mathrm{Osteoid} \underset{k_{-5}}{\overset{k_{+5}}{\rightleftarrows}} \mathrm{New\_B} + D_{15} \qquad (\rho = 5)$$

where D_{13} is the substratum, that initializes mineralization of osteoid, New_B is the abbreviation of new bone formed by remodeling process and D_{15} is the residue of bone formation reaction.

The aforementioned chemicals equations (ρ = 1, 5) described the two most important stages in bone remodeling, i.e., formation and resorption.

Thermodynamic description of bone remodeling process

Bone remodeling as a coupled process of bone resorption and formation can be viewed as an open thermodynamic system that operates far from equilibrium. In this way, nonequilibrium thermodynamic principles developed by Prigogine[29] were applied to describe interactions between the mechanical loading and chemical reactions (Fig. 1).

The second law of equilibrium thermodynamics allows the expression of entropy and the absolute temperature in terms of mechanical ($-p\mathrm{d}V$), chemical ($\mu\mathrm{d}N$), and electrical ($\phi\mathrm{d}q$) contributions etc. The fundamental equation of thermodynamics[30] (i.e., Gibb's equation) in differential form were given by the following equation

$$\mathrm{d}U = T\mathrm{d}\sigma + \mu\mathrm{d}N + p\mathrm{d}V + \phi\mathrm{d}q + \mathrm{etc.}$$

According to the second law of thermodynamics, the entropy production for a living tissue-like bone was always positive and was represented by integrating the aforementioned relationship to obtain[29]

$$T\sigma(S) = pd_{(1)} + w_\rho A_\rho + \sum\nolimits_\alpha j_\alpha.\nabla\mu_\alpha(n_\alpha, p, \phi, \mathrm{etc.}) \geq 0 \qquad (6)$$

where $d_{(1)} = \mathrm{div}(\mathrm{v}) = \frac{\partial \mathrm{v}^1}{\partial x^1} + \frac{\partial \mathrm{v}^2}{\partial x^2} + \frac{\partial \mathrm{v}^3}{\partial x^3} = -\frac{\dot{\rho}}{\rho}$ (i.e., continuity equation) is the rate of deformation tensor, p is a mechanical energy concentration or pressure, w_ρ and A_ρ are the chemical reaction rate and affinity of ρth reaction, respectively. The sum $\sum_\alpha j_\alpha.\nabla\mu_\alpha(n_\alpha, p, \phi, \mathrm{etc.})$ is the rate of entropy production and $j_\alpha(j_q, j_{D\alpha}, j_e,$ etc.) represents the fluxes of chemical component α which include the heat flux ($j_q = -k\nabla T$, Fourier's law), diffusion flux ($j_{D\alpha} = -D\nabla C$, Fick's law) and bioelectrical flux ($j_e = -k\nabla\phi$, Ohm's law).

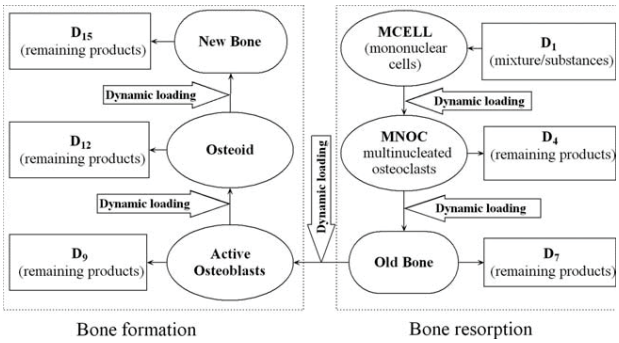

Figure 1. Schematic process of bone remodeling viewed as an open thermodynamic system.

Cowin et al.[31] showed that all fluxes are driven by the gradients of concentrations n_α, pressure p and bioelectrical potential ϕ according to the following relation

$$\left(j_q, j_{D\alpha}, j_e\right)^T = \mathbf{L}(\nabla n_\alpha, \nabla p, \nabla\phi) \qquad (7)$$

where $\mathbf{L}$ is the matrix of phenomenological coefficients. These coefficients must be determined experimentally or estimated on the base of corresponding biophysical models using Onsager symmetrical rules,[32,33] which are similar to Maxwell's relations in thermodynamics.

In the present study, it was assumed that bone remodeling was mainly driven by the interaction between the mechanical and chemical fluxes or forces, thus Eq. (6) was simplified as follows:

$$T\sigma(S) = pd_{(1)} + w_\rho A_\rho \qquad (8)$$

The cross-coupling effects between the pressure (p) and chemical reactions rates (w_ρ) was expressed by Onsager's relations as follows[32,33]

$$p = l_{\mathrm{vv}} d_{(1)} + l_{\mathrm{v}\rho} A_\rho \qquad (9)$$

$$w_\rho = l_{\rho\mathrm{v}} d_{(1)} + l_{\rho\rho} A_\rho \qquad (10)$$

here l_{vv}, $l_{\rho\rho}$ are called direct coefficients related to the viscosity and the chemical reaction rate, respectively, $l_{\mathrm{v}\rho}$, $l_{\rho\mathrm{v}}$ represent the cross coefficients resulting from the coupling. These cross-coefficients must satisfy the Osanger's reciprocal relation, i.e., $l_{\mathrm{v}\rho} = l_{\rho\mathrm{v}}$ and also satisfy the second law of thermodynamics.

By substituting Eqs. (9) and (10) into Eq. (8), Osanger's reciprocal relation and the second law of thermodynamics was satisfied under the following constraints [Appendix D, Eq. (D1)]:

$$l_{\mathrm{vv}} > 0 \quad \text{and} \quad l_{\rho\rho} > 0 \qquad (11)$$

and

$$q = \frac{l_{v\rho}}{\sqrt{l_{vv} l_{\rho\rho}}} \in (-1, 1) \tag{12}$$

where q denotes the coupling parameter.

The role of coupling between mechanical loading and chemical reaction

From the recent analyses of reaction efficiency,[34] the efficiency of interaction H can be defined which describes the "efficiency" of the transformation of chemical energy into mechanical activity.

$$H = \frac{w_\rho A_\rho}{p d_{(1)} + w_\rho A_\rho} \tag{13}$$

To elucidate the role of mechanical loading in remodeling, the dependence of the "efficiency" H on the coupling q was be investigated The ratio of $d_{(1)}$, A_ρ was denoted as

$$\delta = \sqrt{\frac{l_{\rho\rho}}{l_{vv}}} \frac{d_{(1)}}{A_\rho} \tag{14}$$

By replacing Eq. (14) into,[13] the following correlation was obtained

$$H = \frac{\delta q + \delta^2}{1 + 2\delta q + \delta^2} \tag{15}$$

The quantity H serves to estimate the sign of w_ρ. The denominator of Eq. (15) is always positive, due to the second law of thermodynamic [Eq. (8)], therefore the sign of H is equal to the sign of the product $w_\rho A_\rho$.

In nature, all systems, including living tissues, are well optimized.[35] Accordingly, we can assume that the efficiency described by Eq. (15) should have the absolute highest (maximum) value, i.e., $H_{max} = H_{max}(d_{(1)}, A_\rho) = H_{max}(\delta)$.

Positive H_{max} is reached for $\delta = -\frac{1}{q} - \frac{1}{q}\sqrt{1-q^2}$ and the minimal H is reached for $\delta = -\frac{1}{q} + \frac{1}{q}\sqrt{1-q^2}$. H_{max} is negative $\Leftrightarrow -8(1-q^2)^{5/2} + 8 - 20q^2 + 15q^4 - 3q^6 \le 0$ which is satisfied for most values of q ranged between -1 and 1 [Eq. (12)], thus the real effect of chemical reaction is

$$H_{max} = 1 \pm \frac{1}{2} \frac{q^2}{\sqrt{1-q^2}\left(1 \pm \sqrt{1-q^2}\right)} \tag{16}$$

The driving force for all chemical reactions described by equations (ρ = 1–5), which has the general Menten-Michaelis reaction form $\left(\text{i.e., } S \underset{k_-}{\overset{k_+}{\rightleftarrows}} P\right)$ are affinities A_r, which can be positive or negative depending on the values of chemical potentials of products and substrates. For $A_\rho > 0$ (chemical potential of product μ_p is greater than chemical potential of substrate μ_s), the chemical reaction proceeds in the direction $S \to P$ and its rate is $w_\rho > 0$. For the $A_\rho < 0$ (chemical potential $\mu_p - \mu_s \le 0$), the corresponding chemical reaction cannot proceed spontaneously and a positive rate $w_\rho > 0$ is guaranteed only by mechanical loading $l_{\rho v} d_{(1)}$, see Equation (10). Physiological remodeling corresponds to $w_\rho > 0$.

The aforementioned analysis was interpreted as follows:

1 For $A_\rho < 0$, $w_\rho > 0$ the quantity has to be negative $H < 0$, as in Eq. (13). It corresponds to the ratio H_{min}, which is again positive for $-1 < q < 0$ and negative for $0 < q < 1$. In the case of one chemical reaction, any compression $d_{(1)} < 0$ and any expansion $d_{(1)} > 0$ cannot convert the "efficiency" to some positive value. In the case of negative affinity, only mechanical loading cannot drive the chemical reaction. From this consideration, it was evident that inappropriate bone chemistry cannot be replaced by physical exertion.
2 For $A_\rho > 0$, $w_\rho > 0$, the chemical reactions are running spontaneously, and the quantity H is positive. It corresponds to the ratio δ_{max}, which can be both positive (for $-1 < q < 0$) and negative (for $0 < q < 1$). From Eq. (14), it was evident that for expansion $d_{(1)} > 0$ is $\delta_{max} > 0$ (q is negative) and for compression $d_{(1)} < 0$ is $\delta_{max} < 0$ (q is positive). For both cases "efficiency" $H_{max} \ge 1$.
3 With no coupling ($q = 0$, or $d_{(1)} = 0$), there is no cross coefficients effect, which corresponds to $H_{max} = 1$. Hence, it follows that the dynamic loading has a stimulatory effect (i.e., periodic changing of compression and expansion) on remodeling.
4 Bone remodeling is a complex process which involves many chemical reactions. The actual form of the efficiency for the 5 chemical reactions (ρ = 1, 5) is given by

$$H = \frac{\sum_{\rho=1}^{5} w_\rho A_\rho}{p d_{(1)} + \sum_{\rho=1}^{5} w_\rho A_\rho} \tag{17}$$

The reaction may run even in a case when some chemical reactions have negative affinity A_ρ. Then the influence of such reaction $A_\rho w_\rho$ is compensated by the enhanced efficiency of the other reactions.

Kinetics of chemical reactions

Bone is considered to be a self-organizing system (open system) that exchanges matter energy and entropy with its surroundings. Time evolution of the concentrations of all biochemical components of the bone is described by the set of differential equations, which are formulated on the bases of chemical kinetics approach (i.e., Michaelis-Menten reactions[27,28]) and nonequilibrium thermodynamics[29] (Appendix A).

Using the rate law or rate equation for a chemical reaction (i.e., an equation which links the reaction rate with concentrations or pressures of reactants and constant parameters[36,37]), the change of the concentration of chemical substances in the point $x \equiv (x^1, x^2, x^3)$ and time t has the following set of differential equations [Appendix B, Eq. (B1) for the derivation)

$$\frac{d}{dt}[n] = \dot{n}_i = \sum_{\rho=1}^{5} (\nu'_{\rho i} - \nu_{\rho i}) w_\rho \tag{18}$$

where the dot indicates differentiation with respect to time t. i = 1, 2, . . . , 15 and refers to the chemical substances

MCELL, MNOC...,D_7,...,D_{15}, $\nu_{\rho i}$ is the stoichiometrical coefficient of ith chemical component for substrates and $\nu'_{\rho i}$ is the stoichiometrical coefficient of ith chemical component of products.

The system of differential equations (18) can be expressed in dimensionless form by scaling variables utilizing a modified version of the notation used by Ignetik and Deakin,[28] and Heineken et al.[38] [Appendix A, Eq. (A3)].

$$\tau = tk_{+2}n_{B0}, N_i = n_i/n_{B0},\ \delta_\rho = k_{+\rho}/k_{+2},\ \beta_i = B_i/n_{B0},\quad D_\rho = l_{\rho v}d_{(1)}/k_{+2}n_{B0}^2, J_i = j_i/k_{+2}n_{B0}^2 \tag{19}$$

where τ is time, N_i is the rate of concentration of the ith substance, δ_ρ is the ratio of rate of (ρth reaction to second reaction, D_ρ is the parameter that describes the influence of dynamical loading on rate of ρth chemical reaction, β_i is the concentration of the ith substance and n_{B0} is the sum of initial molar concentration of relevant substances and j_i are fluxes of substances, one gets the set of equations[39]

$$\begin{aligned}
\dot{N}_{\mathrm{MCELL}} &= \frac{\partial N_{\mathrm{MCELL}}}{\partial \tau} = -\delta_1(\beta_1 + N_{\mathrm{MCELL}})N_{\mathrm{MCELL}} \\
&\quad + J_3 + J_{\mathrm{New_B}} - D_1, \\
\dot{N}_{\mathrm{Old_B}} &= \frac{\partial N_{\mathrm{Old_B}}}{\partial \tau} = -(\beta_3 - N_{\mathrm{MCELL}} + N_{\mathrm{Old_B}} \\
&\quad + N_{\mathrm{Activ_B}} + N_{\mathrm{Osteoid}} + N_{\mathrm{New_B}})N_{\mathrm{Old_B}} \\
&\quad - \delta_3[\beta_7 - N_{\mathrm{Old_B}} - 2(N_{\mathrm{Activ_OB}} + N_{\mathrm{Osteoid}} + N_{14})]N_{\mathrm{Old_B}} \\
&\quad + 2J_{\mathrm{New_B}} - D_2 - D_3, \\
\dot{N}_{\mathrm{Activ_B}} &= \frac{\partial N_{\mathrm{Activ_B}}}{\partial \tau} \\
&= \delta_3(\beta_7 - N_{\mathrm{Old_B}} - 2(N_{\mathrm{Activ_B}} + N_{\mathrm{Osteoid}} \\
&\quad + N_{\mathrm{New_B)}})N_{\mathrm{Old_B}} - \delta_4(\beta_{10} - N_{\mathrm{Osteoid}} \\
&\quad - N_{\mathrm{New_B}})N_{\mathrm{Activ_OB}} + D_3 - D_4, \\
\dot{N}_{\mathrm{Osteoid}} &= \frac{\partial N_{\mathrm{Osteoid}}}{\partial \tau} = \delta_4(\beta_{10} - N_{\mathrm{Osteoid}} - N_{\mathrm{New_B}})N_{\mathrm{Activ_OB}} \\
&\quad - \delta_5(\beta_{13} - N_{\mathrm{New_B}})N_{\mathrm{Osteoid}} + D_4 - D_5, \\
\dot{N}_{\mathrm{New_B}} &= \frac{\partial N_{\mathrm{New_B}}}{\partial \tau} = \delta_5(\beta_{13} - N_{\mathrm{New_B}})N_{\mathrm{Osteoid}} - J_{\mathrm{New_B}} + D_5,
\end{aligned} \tag{20}$$

Equation (20) admits a positive periodical solution that describes the remodeling [Appendix C, Eq. (C1)]. Time evolution of concentrations of MCELL, Old_B, Activ_B, Osteoid, New_B are determined by solving the kinetic chemical equations (20). The concentrations of all remaining chemical substances (i.e., 15 chemical substances) can be calculated using relations [Appendix B, Eq. (B1)].

Construction of the CAD model of the femur

The bone remodeling algorithm (Fig. 2) described by the system of equations (20) was tested in a standard proximal femur. The idea was to qualitatively simulate bone adaptation due to daily walking activity. Computed tomography (CT) scans of a large, left, synthetic "fourth generation femur" (Model #3306, Pacific Research Labs, Vashon, Washington) were performed at intervals of 0.5 mm along the length of the femur yielded cross-sectional outlines of both cancellous and cortical bones. MIMICS software (Materialise, NV) was used to produce the three-dimensional (3D) geometry of the femoral bone. MMICS allows CT images to be imported for visualization, segmentation, and calculation of 3D objects. Masks were created through specific threshold settings (i.e., min: 1250 and max: 2637) and targeted regions of the femur were selected based on gray values (i.e., density values, see Fig. 3). The masks, which are visible on the corresponding axial, coronal, and sagittal views, were edited in 3D or in individual views so that only the desired regions were selected. Finally, the 3D CAD model of the femur was generated from a desired mask and exported as an initial graphics exchange specification (IGES) file into an FE package.

The original density and the elastic modulus of the simulated cortical (short fiber filled epoxy) and cancellous (rigid polyurethane foam) based on CT scan and ASTM D-638, D-695, D-1621 tests were equal to 1.64 g/cm^3, 16.7 GPa and 0.32 g/cm^3, 137 MPa, respectively. For the numerical simulations, the bone was considered as a linear transversely isotropic material with ($E_x = E_y = 17$ GPa and $E_z = 21$ GPa).[40] The initial density of the composite bone was assumed to be equal to the average value of both bones, i.e., $\rho_0 = (0.32 + 1.64)/2 = 0.98$ (g/cm^3). The material properties of the bone in the first time step depended on the initial value of bone density; in the next time steps the properties changed with bone concentration of old and new bone. A number of case studies have shown that the initial bone density does not have a significant influence on the final density distribution.[41]

Formulation into ANSYS

Calculation of stresses and strains in the bone

The stress fields were calculated using a modified version of Hook's law,[42] that is, the sum of the elastic stress due to elastic deformation (Hook's law) and the dissipative stress due to plastic deformation and viscosity is,

$$\sigma_{ij} = \sigma_{ij}^{(\mathrm{el})} + \sigma_{ij}^{(\mathrm{diss})} \tag{21}$$

The elastic stress follows Hook's law below,

$$\sigma_{ij}^{(\mathrm{el})} = C_{ijkl}\varepsilon_{kl}, 2\varepsilon_{kl} = \frac{\partial u_k}{\partial x^l} + \frac{\partial u_l}{\partial x^k} - \frac{\partial u_m}{\partial x^k}\frac{\partial u_m}{\partial x^l} \tag{22}$$

where C_{ijkl} is the stiffness matrix and ε_{kl} is the tensor of deformations and u is the displacement vector.

Bone was assumed to be a transversely isotropic material, which was defined by five independent elastic constants defined by[43]

$$\begin{aligned}
&c_{1111} = \frac{1 - \nu_{23}\nu_{32}}{E_2E_3\Delta}, c_{2222} = \frac{1 - \nu_{13}\nu_{31}}{E_1E_3\Delta}, c_{3333} = \frac{1 - \nu_{12}\nu_{21}}{E_1E_2\Delta} \\
&c_{1212} = c_{2112} = c_{2121} = c_{1221} = G_{12}, \\
&c_{1313} = c_{3113} = c_{1331} = c_{3131} = G_{31}, \\
&c_{2323} = c_{3223} = c_{2332} = c_{3232} = G_{23}, \\
&c_{3322} = c_{2233} = \frac{\nu_{32} + \nu_{12}\nu_{31}}{E_1E_3\Delta} = \frac{\nu_{23} + \nu_{21}\nu_{13}}{E_1E_3\Delta} \\
&c_{1122} = c_{2211} = \frac{\nu_{21} + \nu_{31}\nu_{23}}{E_2E_3\Delta} = \frac{\nu_{12} + \nu_{32}\nu_{13}}{E_1E_3\Delta} \\
&\Delta = \frac{1 - \nu_{12}\nu_{21} - \nu_{23}\nu_{32} - \nu_{31}\nu_{13} - 2\nu_{21}\nu_{32}\nu_{13}}{E_1E_2E_3}
\end{aligned} \tag{23}$$

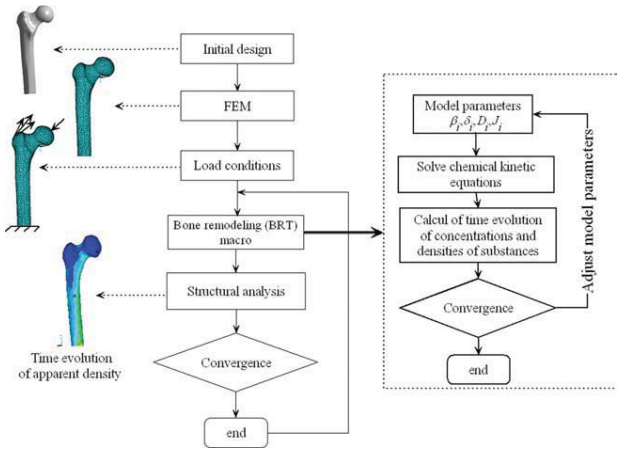

Figure 2. Iterative process of the thermodynamic bone remodeling. [Color figure can be viewed in the online issue, which is available at wileyonlinelibrary.com.]

The dissipative stress due to viscosity and plasticity follows Eq. (9) and was,

$$\sigma_{ij}^{(\mathrm{diss})} = \mu_{\mathrm{v}} d_{(1)} + \sum l_{\mathrm{v}\rho} A_{\rho} \tag{24}$$

Because bone is a dynamic living tissue that updates its structure to the applied load, the stiffness matrix coefficients are not constant but vary with the dynamic load and the concentration of the old and new bone [see Eq. (31)]

$$C_{ijkl} = C_{ijkl}[\mathrm{Old\_B}, \mathrm{New\_B}] = C_{ijkl}\left[\mathrm{Old\_B}\left(d_{(1)}\right), \mathrm{New\_B}\left(d_{(1)}\right)\right] \tag{25}$$

To find the relationship between the elastic constants and the constants of old and new bone, the total stress-strain in the bone must be expressed as a function of the concentrations. If the elastic constants of old bone (OB) were denoted by $C_{ijkl}(\mathrm{OB})$ and its deformation by $\varepsilon_{kl}(\mathrm{OB})$, then the stress undertaken by the old bone was

$$\sigma_{ij}(\mathrm{OB}) = C_{ijkl}(\mathrm{OB})\varepsilon_{kl}(\mathrm{OB}) \tag{26}$$

Analogously, the stress for the new bone was

$$\sigma_{ij}(\mathrm{OB}) = C_{ijkl}(\mathrm{OB})\varepsilon_{kl}(\mathrm{OB}) \tag{27}$$

The total stress in the bone was given by

$$\begin{aligned}\sigma_{ij} &= \sigma_{ij}(\mathrm{OB}) + \sigma_{ij}(\mathrm{NB}) = C_{ijkl}(\mathrm{OB})\varepsilon_{kl}(\mathrm{OB}) + C_{ijkl}(\mathrm{NB})\varepsilon_{kl}(\mathrm{NB}) \\ &= \left(C_{ijkl}(\mathrm{OB})\frac{\varepsilon_{kl}(\mathrm{OB})}{\varepsilon_{kl}} + C_{ijkl}(\mathrm{NB})\frac{\varepsilon_{kl}(\mathrm{NB})}{\varepsilon_{kl}}\right)\varepsilon_{kl}\end{aligned} \tag{28}$$

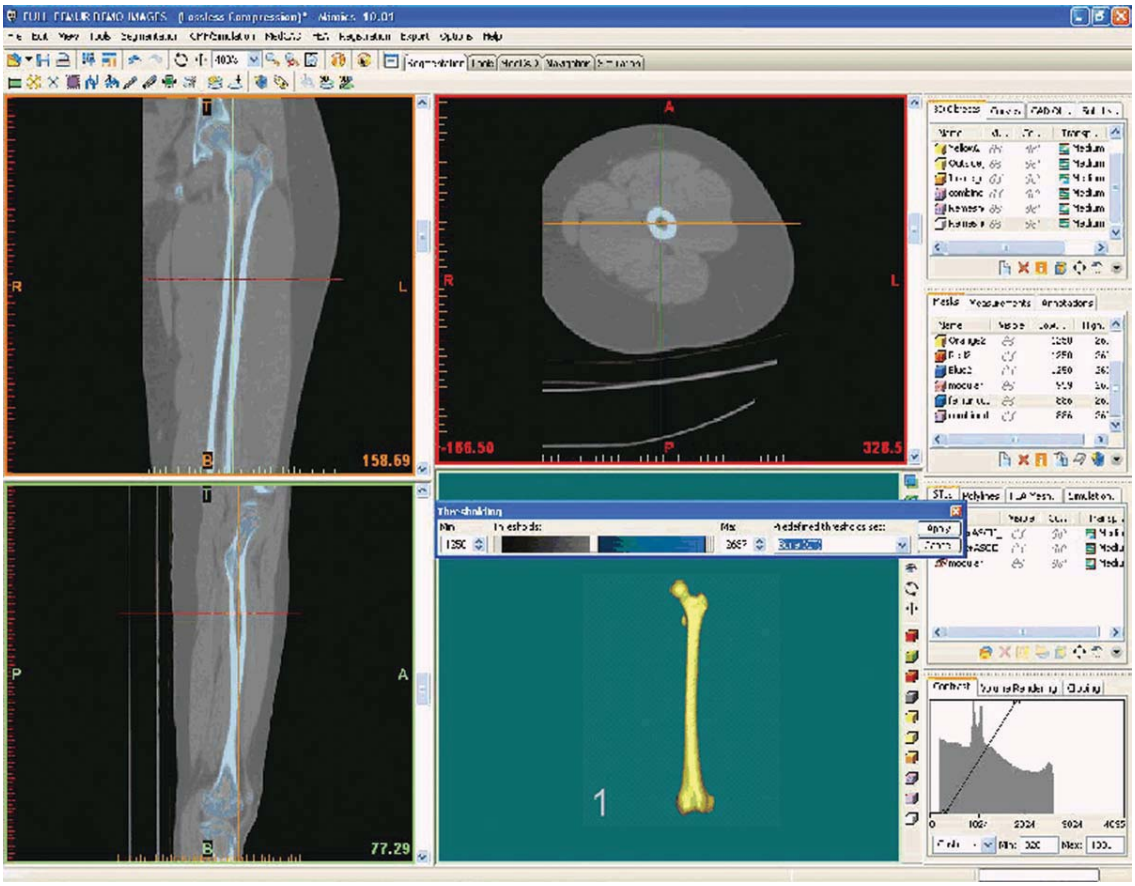

Figure 3. Generation of the 3D geometry of the femur from CT scans using MIMICS. [Color figure can be viewed in the online issue, which is available at wileyonlinelibrary.com.]

From Eq. (26) a plausible assumption between the concentrations and the deformation was drawn from load sharing rule[43]

$$\frac{\varepsilon_{kl}(\mathrm{OB})}{\varepsilon_{kl}} \propto \frac{\frac{n_{\mathrm{OB}}}{n} V^*_{\mathrm{OB}}}{\frac{n_{\mathrm{OB}}}{n} V^*_{\mathrm{OB}} + \frac{n_{\mathrm{NB}}}{n} V^*_{\mathrm{NB}}}, \frac{\varepsilon_{kl}(\mathrm{NB})}{\varepsilon_{kl}} \propto \frac{\frac{n_{\mathrm{NB}}}{n} V^*_{\mathrm{NB}}}{\frac{n_{\mathrm{OB}}}{n} V^*_{\mathrm{OB}} + \frac{n_{\mathrm{NB}}}{n} V^*_{\mathrm{NB}}} \tag{29}$$

with $n = n_{\mathrm{OB}} + n_{\mathrm{NB}}$.

Equation (29) means that the ratios of the components of the deformation tensor reflect more volume fraction. V^*_{OB} and V^*_{NB} were the molar volumes of the old and new bone respectively. The concentrations n_{OB}, n_{NB} were calculated from the biochemical model [Eq. (20)].

By replacing Eq. (29) into Eq. (28), the relationship was obtained between the stress-strain and the concentrations of old and new bone, as follows,

$$\sigma_{ij} = \left(C_{ijkl}(\mathrm{OB}) \frac{\frac{n_{\mathrm{OB}}}{n} V^*_{\mathrm{OB}}}{\frac{n_{\mathrm{OB}}}{n} V^*_{\mathrm{OB}} + \frac{n_{\mathrm{NB}}}{n} V^*_{\mathrm{NB}}} + C_{ijkl}(\mathrm{NB}) \frac{\frac{n_{\mathrm{NB}}}{n} V^*_{\mathrm{NB}}}{\frac{n_{\mathrm{OB}}}{n} V^*_{\mathrm{OB}} + \frac{n_{\mathrm{NB}}}{n} V^*_{\mathrm{NB}}} \right) \varepsilon_{kl} \tag{30}$$

The elastic constant of the bone were

$$C_{ijkl} = C_{ijkl}(\mathrm{OB}) \frac{\frac{n_{\mathrm{OB}}}{n} V^*_{\mathrm{OB}}}{\frac{n_{\mathrm{OB}}}{n} V^*_{\mathrm{OB}} + \frac{n_{\mathrm{NB}}}{n} V^*_{\mathrm{NB}}} + C_{ijkl}(\mathrm{NB}) \frac{\frac{n_{\mathrm{NB}}}{n} V^*_{\mathrm{NB}}}{\frac{n_{\mathrm{OB}}}{n} V^*_{\mathrm{OB}} + \frac{n_{\mathrm{NB}}}{n} V^*_{\mathrm{NB}}} \tag{31}$$

Calculation of density and elastic moduli of the bone

The density in each element of the bone is related to the initial density and the normalized concentrations of the new and old bone according to the following law of mass and mixture[36]

$$\rho(I) = \rho_0 (N_{\mathrm{Old\_B}}(I) + N_{\mathrm{New\_B}}(I)) \tag{32}$$

In each element, the elastic modulus was updated using an amended version of the empirical power law relationship proposed previously by Carter et al.[44]

$$E(I) = \left(E_{\mathrm{Old}} \left[\frac{N_{\mathrm{Old\_B}}}{N_{\mathrm{Old\_B}} + N_{\mathrm{New\_B}}} \right] + E_{\mathrm{New}} \left[\frac{N_{\mathrm{New\_B}}}{N_{\mathrm{Old\_B}} + N_{\mathrm{New\_B}}} \right] \right) \left(\frac{\rho(I)}{\rho_0} \right)^3 \tag{33}$$

The aforementioned Eqs. (32) and (33) for calculating the updated material properties differed substantially from existing experimental and empirical relationships.[45–48] These relationships are well documented by Helgason et al.[49]

Calculation of the dynamic loading

ANSYS FE calculates only the deformation (i.e., sum of principal strains also known as the trace of the strain) and stresses in each element of bone. To determine the rate of the deformation tensor $d_{(1)}$ (i.e., strain rate), the deformation $\varepsilon_{(1)}$ with respect to time t must be derived,

$$d_{(1)}(I) = \frac{d\varepsilon_{(1)}(I)}{\mathrm{d}t} \approx \frac{\Delta\varepsilon_{(1)}(I)}{\Delta t} \approx \frac{\varepsilon_{(1)}(I)}{\Delta t} \tag{34}$$

where $\varepsilon_{(1)}(I)$ is the trace of the strain (i.e., sum of the principal strains) in the element (I). Δt is the time of loading. Equation (34) includes the influence of frequency of loading on bone remodeling. This frequency of loading is proportional to the strain rate ($d\varepsilon_{(1)}(I)/\mathrm{d}t$) and thus inversely proportional to $\mathrm{d}t$. Torcasio et al.[50] provide a more detailed explanation of the relationship between strain rate and frequency.

As constants defining the model parameters are more or less still unknown ($k_{\pm\rho}$, rate of chemical reactions; N_i, normalized concentrations of several substances), it can be assumed based on Hook's law, that a linear relationship exists between the influence of the strain rate on the ρth chemical reaction D_ρ and the rate of the deformation tensor $d_{(1)}$

$$D_\rho(I) = C d_{(1)}(I) = C \frac{\varepsilon_{(1)}(I)}{\Delta t} \tag{35}$$

where C is a constant, which can be defined similarly to Huiskes reference strain relationship,[7] as the ratio of the influence of the reference strain rate on the ρth chemical reaction and the reference strain rate is,

$$C = \frac{D_\rho(\mathrm{ref})}{S(\mathrm{ref})} \tag{36}$$

The reference strain distribution was found by performing an FE analysis of the intact femur (site-specific remodeling rule[4,24]). The physiological strain and strain rate for the bone (i.e., references values) are between 3000 and 4000 μstrain and between 0.01 and 0.1 s^{-1}, respectively.[51] Values of 3500 μstrain and 0.05 s^{-1} were used in the present FEA.

As the dynamic loading is always positive, the combination of Eqs. (35) and (36) led to

$$\mathrm{D}_\rho(I) == \frac{1}{\Delta t} \frac{|\varepsilon_{(1)}(I)|}{S(\mathrm{ref})} \mathrm{D}_\rho(\mathrm{ref}) \tag{37}$$

In case the strain rate is equal to the reference strain rate then $D_\rho(I) = D_\rho(\mathrm{ref})$

$$\mathrm{D}_\rho(I) = \frac{|d_{(1)}(I)|}{S(\mathrm{ref})} D_\rho(\mathrm{ref}) = \frac{1}{\Delta t} \frac{|\varepsilon_{(1)}(I)|}{S(\mathrm{ref})} \mathrm{D}_\rho(\mathrm{ref}) \tag{38}$$

The absolute value of dynamic load was used because the compressive load is always followed instantly by an expansion and the tensile one by reduction. Thus, both types of load (i.e., compression and tension) may have the same effect on bone remodeling.[51] This can be explained by the fact the production of entropy always has to be positive.

RESULTS

Verification of the thermodynamic bone remodeling model

A numerical code was generated in both MATLAB and ANSYS software to solve the bone remodeling

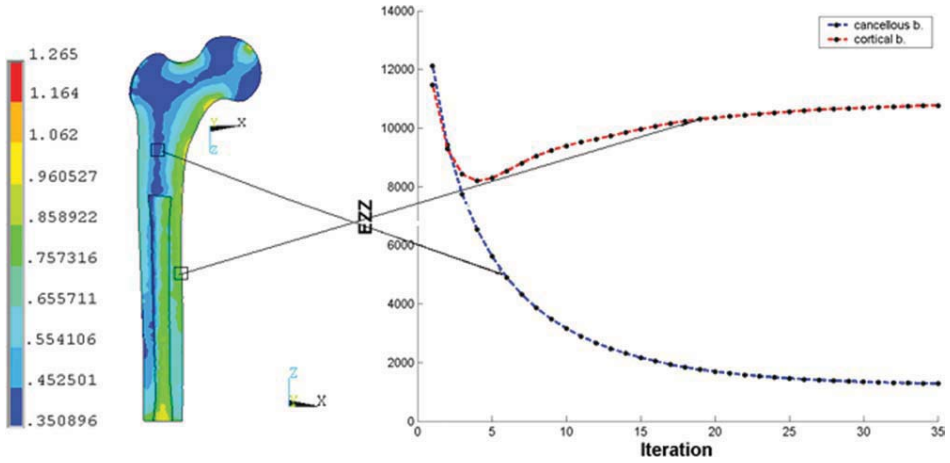

Figure 4. Time evolution of the elastic modulus in z direction (E_{ZZ}) in two different zones of the femoral bone versus the number of iteration. [Color figure can be viewed in the online issue, which is available at wileyonlinelibrary.com.]

process describing the system of differential equations (20). The iterative process started from a constant bone density and ended with variable density at the equilibrium state. The equilibrium state was obtained when the time evolution of properties (i.e., density and elastic modulus) remained unchanged. Figure 4 represented the time evolution of the elastic modulus in the longitudinal direction (direction of osteons, E_{ZZ}) in two different zones of the bone versus the number of iterations (N). As can be seen, values of (E_{ZZ}) decreased with the increase of (N) and the steady state was reached after 40 iterations.

To verify the efficiency of FE model, the current bone configuration was compared to the frontal longitudinal midsection of upper femur from clinical observation.[52] Prediction of bone density in the composite femur using the BRT model [Fig. 5(b)] showed a good agreement with X-rays of a healthy femur [see Fig. 5(a)]. The development was seen of dense cortical bone around the medullary canal and dense trabeculæ bone between the femoral head and the calcar region of the medial cortex due to compressive stresses.

The thermodynamic model was also compared with the classical adaptive bone remodeling model developed previously and Weinans et al.[4] and used by some of the authors to investigate bone remodeling in a new biomimetic hip prosthesis.[24] This model used the strain energy density (SED) as the mechanical stimuli that launches and controls bone remodeling process. By comparing bone density distributions using both models (i.e., strain energy and thermodynamic based models; Fig. 6), the architecture of the femoral bone was, in general, found comparable. The clear formation was noticed of cortical and cancellous bone in both models. However, the main difference was observed in the range of values of bone density in the proximal part of the femur. This may be due to the boundary conditions used in the classical model. For instance, values of starting and ending points for the predicted apparent density were constant in the strain energy based model, (i.e., the apparent density varied between 00.1 and 1.74 g/cm^3).[4,7] In the thermodynamic model, these limits vary with the bone metabolism (i.e., the initial bone concentration, chemical rates etc.). However, this difference may also be attributed to the fact that the strain energy based model considered the strain as the driving force for bone remodeling process [Eq. (22)], but the thermodynamic model considered both the strain rate and the chemical affinity [see Eq. (24)].

Simulation of bone remodeling reality

To simulate the reality of bone remodeling model, a normalized time for normal walking was approximated by a stepwise function [Fig. 7(a)]. These steps represented the mean values of dynamic loading. This approximation for normal walking was based

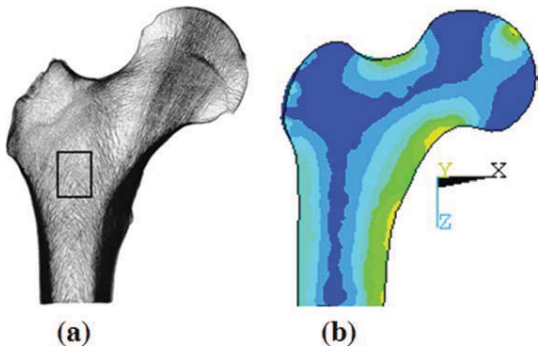

Figure 5. Inner structure of the proximal femur, (a) X-ray of a natural femur, (b) structure of the composite femur predicted by the TBR model. [Color figure can be viewed in the online issue, which is available at wileyonlinelibrary.com.]

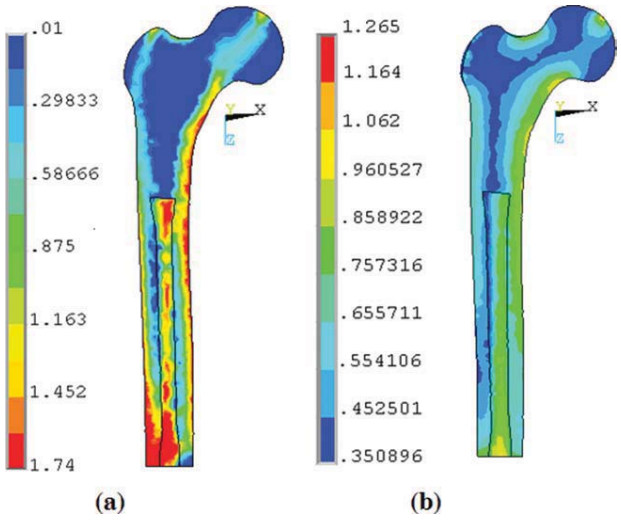

Figure 6. Bone density distribution in the femur using: (a) strain energy-based model and (b) thermodynamic-based model. [Color figure can be viewed in the online issue, which is available at wileyonlinelibrary.com.]

on time transformation estimation of changes in bone. The bone remodeling cycle was assumed to last ~250 days.[25] According to the current model, changes in bone became evident in roughly 25–50 days which corresponded to reality.[53] Time evolution of concentration of old and new bone were presented in Figure 7(b), which shows how remodeling process proceeds in the human body as an open thermodynamic system.

Effect of mechanical loading

Most studies agreed that dynamical loading plays a crucial role in bone remodeling.[53] In this investigation, only the five parameters describing the influence of the dynamic loading (D_ρ, $\rho = 1,\ldots5$) were assumed to vary throughout the bone. All the other parameters were assumed to be constant throughout the whole bone and independent of time. All the calculated results for the effect of mechanical loading are a consequence solely of dynamic loading as a control factor.

The effect of the dynamic loading on bone density is shown in Figure 8. The bone density increased with the mechanical loading. However, without mechanical loading, the bone was partially lost and reached a new steady state after about 50%. Notice that bone loss was not complete; this means that in the absence of mechanical stimuli bone maintenance was driven by other mechanisms including metabolic factors (chemical and biological) and/or other external contributions such as nutrition. This was consistent with an animal study on immobilized dog bones, indicating that after a prolonged period of disuse, trabecular bone was rapidly lost and reached a new steady state after about 50% bone loss.[54]

Figure 9 showed the upper and lower limits of mechanical loading. These upper and lower limits were obtained for the following values of the influence of dynamic loading, $D_{\rho=1,\ldots,5} = 6$ and $D_{\rho=1,\ldots,5} = 0.3$, respectively. As can be seen, inadequate dynamic loading (e.g., excessive loading or small loading) led to either bone densification or bone resorption, which may in turn increase the risk of bone fracture. Several clinical studies showed that bone stress fractures could result from excessive loading.[55] In addition, other clinical studies confirmed that, after hip arthroplasty, higher load could cause bone densification around the distal tip of the implant and possible fracture in the patient femur may occur.[56,57]

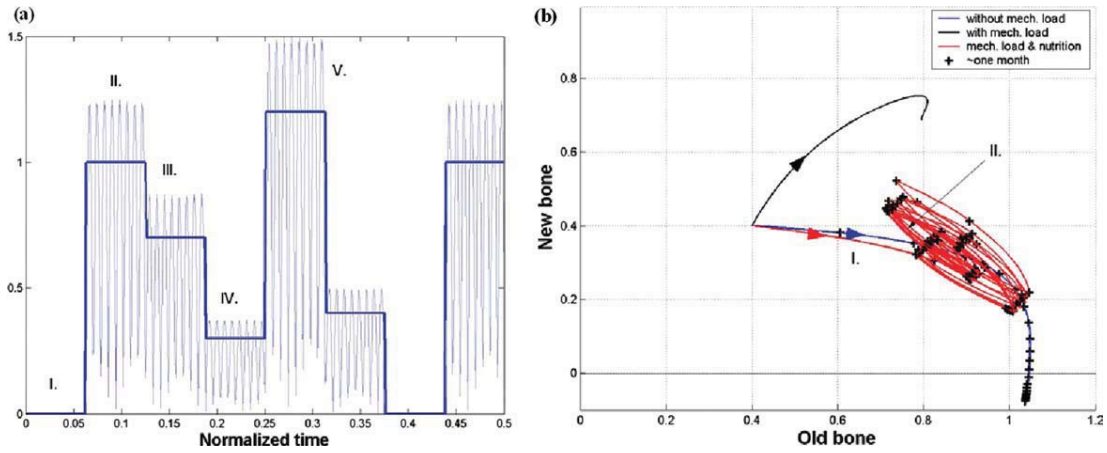

Figure 7. Approximation of reality of bone remodeling: (a) normalized time for walking and (b) time evolution of bone density (new bone versus old bone). [Color figure can be viewed in the online issue, which is available at wileyonlinelibrary.com.]

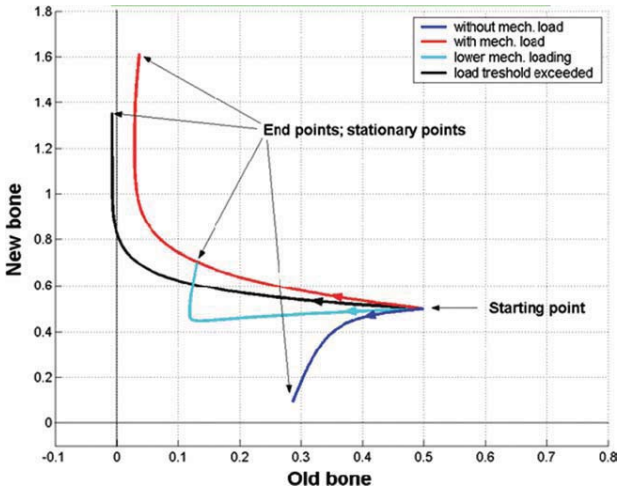

Figure 8. Effect of dynamical loading on bone density. [Color figure can be viewed in the online issue, which is available at wileyonlinelibrary.com.]

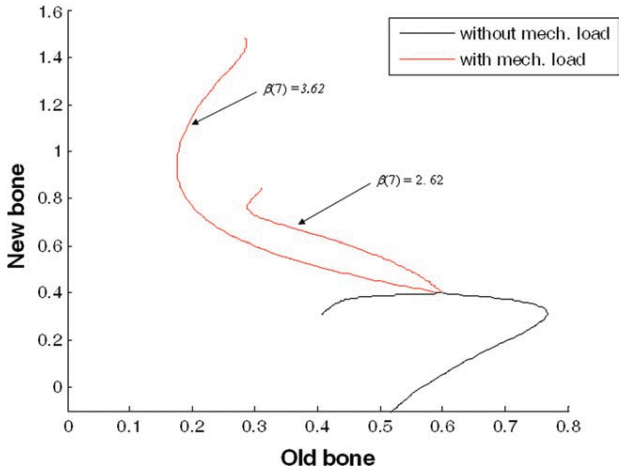

Figure 10. Effect of metabolic factor β_7 on bone density. [Color figure can be viewed in the online issue, which is available at wileyonlinelibrary.com.]

Effect of some metabolic factors (concentrations of active osteoblasts and osteoid)

To illustrate the effect of some metabolic factors, the concentrations of the 7th and 10th substances, β_7 and β_{10}, were chosen which corresponded to the concentrations of active osteoblast and osteoid, respectively. These concentrations represent the sum of corresponding initial concentrations. For instance, the concentration of osteoid is $\beta_{10} = n_{10,0} + n_{11,0} + n_{14,0}$ [see Appendix B, Eq. (B1)]. Their respective effects on bone concentration are presented in Figures 10 and 11. As can be seen, the concentrations of old bone and new bone are very sensitive to the variation of β_7 and β_{10}. In the absence of dynamic loading, the bone is rapidly lost and reaches a new steady state after ~50% bone loss for β_7 =2.62. However, increasing β_7 from 2.62 to 3.62 restore bone loss. This means that an increase in active osteoblast concentration implies an increase in bone deposition and therefore prevents bone from resorption.[58] The total bone concentration (i.e., some of the concentration of old bone and new bone) at the steady state is approximately equal to 0.75. In the case of dynamic loading, the increase of β_7 increases the concentration of bone from 1.17 to 1.79 (i.e., ~35% increase in bone concentration). Figure 10 shows the effect of β_{10} on the bone concentration. In the case of dynamic loading, increasing β_{10} from 2.28 to 3.28, increases the concentration of bone by ~15%. The effect of β_{10} on bone concentrations is less pronounced than the effect of β_7, which may be explained by the fact that the mineralized volume is much bigger (by ~4 times) than the osteoid volume.[9]

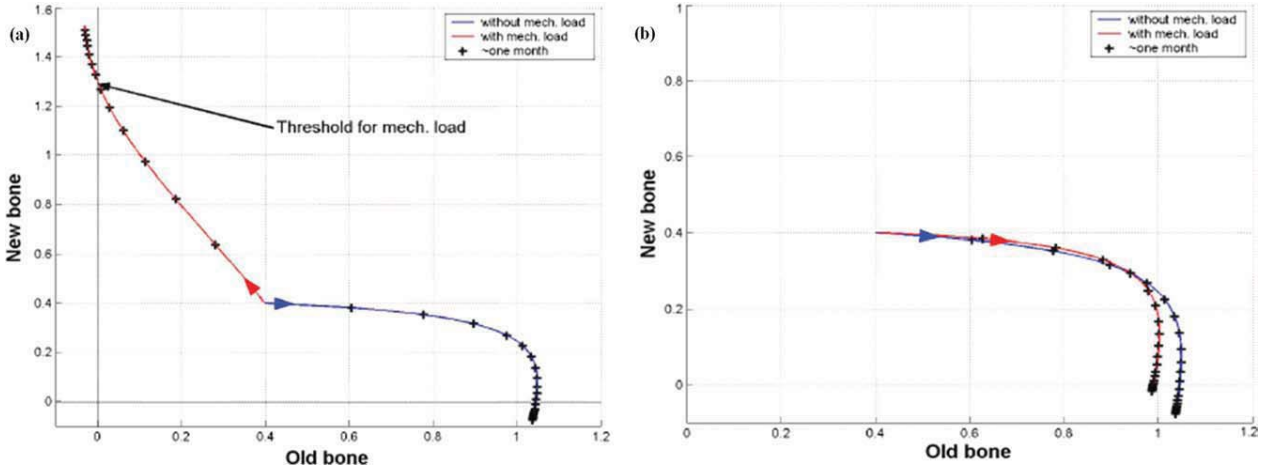

Figure 9. (a) Upper and (b) lower limits of dynamic loading. [Color figure can be viewed in the online issue, which is available at wileyonlinelibrary.com.]

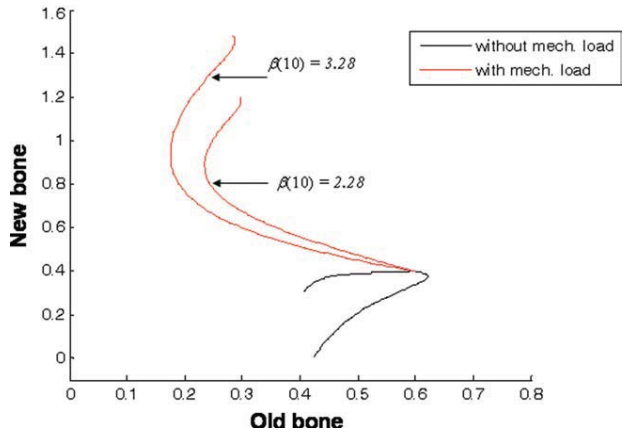

Figure 11. Effect of metabolic factor β_{10} bone density. [Color figure can be viewed in the online issue, which is available at wileyonlinelibrary.com.]

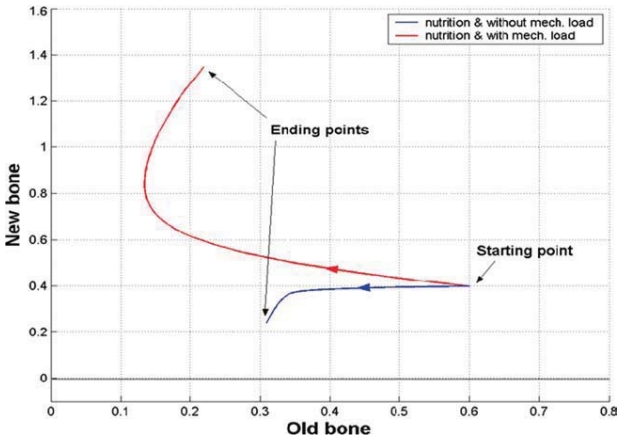

Figure 13. Influence of nutrition on bone remodeling. [Color figure can be viewed in the online issue, which is available at wileyonlinelibrary.com.]

Effect of the frequency of loading

It is known that, for example, swimming is not nearly as good as walking as a stimulus for bone remodeling.[59,60] The frequency of loading is proportional to the strain rate.[50] To illustrate the effect of activity on bone remodeling, a smaller frequency corresponding to Δt = 7s was compared to the one corresponding to Δt = 1s. As shown in Figure 12, decrease of frequency resulted in significant decrease in density throughout the whole bone and likely higher strain occurred.[44,61,62] At Δt = 1s, the bone density of the new bone (at the ending point) is ~1.26 g/cm^3, however, this value drops to 0.8 g/cm^3 when Δt = 7s. A recent clinical study in young women with low bone mineral density (BMD) has shown that high-frequency mechanical signals are likely to enhance bone mass and extremely low-frequencies are anabolic to bone tissue.[63] Another clinical study also revealed that high-impact exercise (high strain rates or frequencies) enhanced bone formation.[59]

Effect of nutrition

Several prior studies show that nutrition (e.g., vitamin D) plays an important role in the maintenance of bones.[64,65] Vitamin D is essential in the development of an intact and strong skeleton, and it promotes bone formation and mineralization. Kitazawa et al.[66] and Watson et al.[67] showed that in the case of continuous release of parathyroid hormone (PTH) a net increase in bone resorption and osteoblast and osteoclast concentrations were observed. As bone remodeling is primed by PTH as well as vitamin D,[68] it can be supposed that nutrition acts directly on osteoblast and osteoclast concentrations of Eqs. (1) and (5), precisely on β_1 and β_{13}. To simulate the effect of nutrition on bone remodeling, a constant rate for nutrition equal to concentration β_1 (i.e., 1.23/day) was assumed. Adding some nutrition can impact bone density, especially on the lower limit (end points) of bone density (see Fig. 13). In the case of absence of both nutrition and mechanical

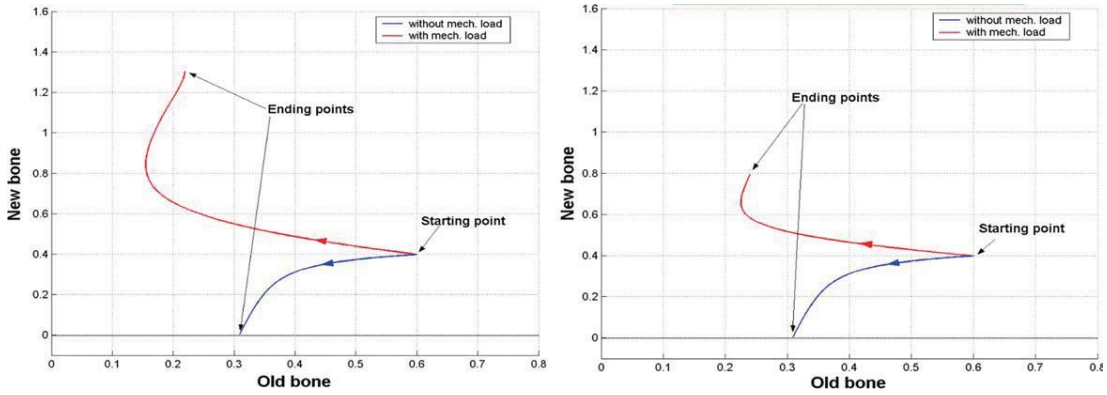

Figure 12. Effect of frequency of loading: (a) time evolution of bone density with normal frequency and (b) with 7 times smaller frequency. [Color figure can be viewed in the online issue, which is available at wileyonlinelibrary.com.]

loading, the lower limit of bone density (i.e., the sum of old bone and new bone) was 0.31 g/cm^3 [Fig. 12(a)]. However, when nutrition was added, new bone was formed and the value of the lower limit is 0.53 g/cm^3 [0.31 (old bone) + 0.22 (new bone)], which is an increase of 41.5% in bone density. This increase in bone density predicted by the thermodynamic model is comparable to some clinical studies on the effect of PTH on bone cells.[68,69] One study using cells from rat calvaria showed that consistent administration of PTH increased calcium uptake about 30–40% of the control value,[68] while the second study on the effect of parathyroid hormone-related peptide (PTHrP) on osteoblast-like cell line found an increase in cell number by 50%.[69]

DISCUSSION

In this study, a novel model for bone remodeling based on irreversible thermodynamics principles was proposed. The model linked metabolic factors to mechanical ones using irreversible thermodynamics. This model calculated the time evolution of bone properties (i.e., molar concentrations and young modulus in different parts of bone). It was applied first to simulate time evolution of bone density in a healthy femur.

There are several bone adaptation theories (remodeling models), but a large portion of these theories is based on the influence of mechanical load.[5–7,62,70,71] Some of these models suggested that in the absence of stress, bone will resorb completely. This statement disagrees with *in vivo* observances. When limbs are placed in casts (i.e., the bone loading is minimal), bone is rapidly lost and reaches a new steady state after about 50% bone loss.[54] On the other hand, there are a few biological cell-based models[12] for bone regulation, but they neglecting the effect of mechanical stimulus, which is known to play an important role in bone remodeling. Another model which takes into account biochemomechanical affinity was recently proposed by Rouhi et al.[11] This model is intended for bone resorption and could be extended to bone adaptation and growth according to the authors.

Numerical simulations of bone density distributions roughly agreed with X-rays of a healthy femur and with results obtained using the strain energy model. The proposed thermodynamic bone remodeling (TBR) model suggested the existence of a relationship between the dynamic loading and chemical reaction which induces change in bone tissue density as prescribed by nonequilibrium thermodynamics. Contrary to some continuum-based models, which state that without mechanical stimulus bone is completely resorbed.[4,7,61,72] The current model suggested that in the absence of mechanical stimuli, bone is par partially resorbed and bone remodeling is driven by metabolic factors and external contributions such as nutrition. This is consistent with clinical observation.[54] The model also suggests that lower frequencies decrease bone density, thus according to the model weak bones under low frequencies may be prone to fracture. This claim is supported by evidence from the literature.[63] In addition, the model showed that metabolic factors such as the sum of initial concentrations of active bone and osteoid (e.g., β_7 and β_{10}) play an important rule in preventing from bone loss and promoting the formation of new bone. This is consistent with previous study on the multiple effects of metabolic factors on bone cell proliferation and differentiation rates.[12,68,73]

Limitations of the model

The proposed model was originally intended as a simplified model of bone metabolism remodeling, which includes only two stages, i.e., bone formation and resorption. Although this simplified model presents many features of bone remodeling in comparison with classical models, the main limitation of the TBR model is caused by the difficulty to adjust different parameters (biochemical ones). The values of these parameters which characterize the chemical reactions are not known, and in order to obtain them experimental measurements are needed. For instance, the characteristic time of the mechanical stimuli, which is included in the metabolic constant k_ρ and is equal to $\sim 10^{-8}$ s, was measured using a microfluidic model developed by Schmidt et al.,[74] in which the pressure wave propagation in bone fluid with a speed of sound and a geometrical dimension of $\sim$1500 m/s and 10 nm, respectively were used.

The partial solution of this problem (i.e., values of different parameters such as chemical concentrations of substances) may be found in comparing calculated results for a given set of parameters with real data from clinical observation and adjusting them accordingly. Another limitation in this study is the fact that only two metabolic factors were varied throughout the bone. As mentioned earlier, this limitation is due to the lack of information about these metabolic parameters and also the difficulty to adjust them. Further research (both experimental and numerical) is needed to determine the values of these parameters and improve the model accordingly. Nevertheless, this simplified model is the first step in the development of a new framework for bone remodeling based on nonequilibrium thermodynamics. The preliminary results obtained (i.e., patterns of bone density) as well as the model's features (e.g., dynamic loading, frequency of load and nutrition)

were generally comparable to the literature and clinical observation.[7,54,68,69]

CONCLUSIONS

Bone remodeling is a complex process which involves interactions between mechanical, chemical, and biological parameters. In this investigation, a new thermodynamic-based model for bone remodeling was presented. The model took into account the interaction between mechanical and biochemical factors involved in the process of bone remodeling. Irreversible thermodynamics and chemical kinetics were used to derive the mathematical equations governing this process. This preliminary model provides valuable information about the time evolution of the bone properties (e.g., bone density and elastic modulus), the effect of mechanical loading and some metabolic factors, as well as nutrition and frequency of loading. A modified version of this preliminary thermodynamic model was used in a related study to predict the functional adaptation of bone after total hip replacement surgery.[23] The evolution of the bone density calculated by the thermodynamic model was comparable to that shown in clinical data.

APPENDIX A

Michaelis-Menten reaction

The irreversible Michaelis-Menten scheme is given by the following relation

$$E + S \underset{k_{-1}}{\overset{k_{+1}}{\rightleftarrows}} C \xrightarrow{k_2} E + P \tag{A1}$$

where E is the enzyme, S is the substrate, C is the enzyme-substrate complex, P is the product and k_i ($i = -1, 1, 2$) are the rate coefficients.

The kinetic approach to the Michaelis-Menten mechanism of enzyme reactions leads to the following equations

$$\begin{aligned}
&\frac{d[S]}{dt} = -k_1[E_0][S] + (k_1[S] + k_{-1})[C] \\
&\frac{d[C]}{dt} = k_1[E_0][S] - (k_1[S] + k_{-1} + k_2)[C] \\
&\frac{d[P]}{dt} = k_2[C] \\
&[E] + [C] = [E_0] \\
&[S] + [C] + [P] = [S_0],
\end{aligned} \tag{A2}$$

where square brackets [] denote concentrations, $[E_0]$ and $[S_0]$ are the initial concentrations of enzymes and substrate, respectively, and t is the time.

Egnetik and Deakin[28] put these equations into a dimensionless form using a slightly modified version of Heineken et al.[38]

$$\begin{aligned}
&\tau = k_1[E_0]t, y = {}^{[S]}\!/_{[S_0]}, z = [C]/[E_0], \\
&\mu = {}^{[E_0]}\!/_{[S_0]}, \nu = k_2/(k_1[S_0]), \eta = k_{-1}/(k_1[S_0]),
\end{aligned} \tag{A3}$$

The differential equation become

$$\begin{aligned}
&\dot{y} = -y + (y + \eta)z \\
&\mu\dot{z} = y - (y + \nu + \eta)z,
\end{aligned} \tag{A4}$$

where the dot indicates differentiation with respect to τ.

APPENDIX B

Model's assumptions

1. Fluxes of substances, J_i, are constant in time
2. Existence of stationary solution
3. Linear relations among fluxes
4. Remodeling is carried out by the cooperation of osteoclasts and osteoblasts that are formed in a "cutting cone." These brigades are attracted to specific site by some local factors, which are created only when needed. Thus, remodeling does not need to run in every element simultaneously.
5. In the present model, it is assumed that it actually proceeds in every element, but over time each iteration shows that the formal difference vanishes.

Concentration of all remaining substances

Based on the definition of the reaction rate,[37] the reaction rates for equations ($\rho = 1, 5$) can be written as follows

$$\begin{aligned}
&\rho = 1 \rightarrow \text{merge of osteoclasts}, \\
&\qquad w_1 = k_{+1}n_1n_2 - k_{-1}n_3n_4 + l_{1v}d_{(1)} \\
&\rho = 2 \rightarrow \text{resorption of osteoblasts}, \\
&\qquad w_2 = k_{+2}n_3n_5 - k_{-2}n_6 \\
&\rho = 3 \rightarrow \text{activation of osteoblasts}, \\
&\qquad w_3 = k_{+3}n_2n_5 - k_{-3}n_7n_8 + l_{3v}d_{(1)} \\
&\rho = 4 \rightarrow \text{merge of osteoid}, \\
&\qquad w_4 = k_{+4}n_7n_9 - k_{-4}n_{10}n_{11} \\
&\rho = 5 \rightarrow \text{deposition of new bone}, \\
&\qquad w_5 = k_{+5}n_{12}n_{10} - k_{-5}n_{13}n_{14}
\end{aligned} \tag{B1}$$

The concentrations of all remaining chemical substances are calculated using the following relations[39]

$$\begin{aligned} n_1 &= \beta_1 + n_2 \\ n_3 &= \beta_3 - n_2 + n_5 + n_8 + n_{11} + n_{14} \\ n_7 &= \beta_7 - n_5 - 2n_8 - 2n_{11} - 2n_{14} \\ n_{10} &= \beta_{10} - n_{11} - n_{14} \\ n_{13} &= \beta_{13} - n_{14} \end{aligned} \tag{B1}$$

where β_i are sum of corresponding initial concentrations (e.g., $\beta_{10} = n_{10,0} + n_{11,0} + n_{14,0}$).

APPENDIX C

Model analysis

To have a concept of solution behavior, it is useful to examine the existence and stability of stationary solutions.[75] If the rate of the forward reaction is assumed to be much greater that the backward rate (i.e., $k_{+r} \gg k_{-\rho}$, ($k_{+\rho} \gg k_{-\rho}$, $\forall\rho$)), it is possible to find a stationary solution. In addition, if we realize that all normalized concentrations (N_i) should be positive (therefore stationary solutions will exist too), then there will be at most one fixed point corresponding to[39]

$$\begin{aligned} N_{\mathrm{MCELL}} &= 1/2\left(-\beta_1 + \sqrt{\beta_1^2 + 4\frac{-\mathrm{D}_1 + J_3 + J_{14}}{\delta_1}}\right) \\ N_{\mathrm{Old\_B}} &= 1/2\left[-(\beta_7 + 2\beta_3 - 2N_{\mathrm{MCELL}}) + \sqrt{(\beta_7 + 2\beta_3 - 2N_{\mathrm{MCELL}})^2 + 4\left(\frac{J_{14} - \mathrm{D}_3}{\delta_3} + 2(J_{14} - \mathrm{D}_2)\right)}\right] \\ N_{\mathrm{Activ\_B}} &= 1/2\left[-\left(\beta_{10} + \frac{1}{2}\left(N_{\mathrm{Old\_B}} - \beta_7 + \frac{J_{14} - \mathrm{D}_3}{\delta_3 N_{\mathrm{Old\_B}}}\right)\right) + \sqrt{\left(\beta_{10} + \frac{1}{2}\left(N_{\mathrm{Old\_B}} - \beta_7 + \frac{J_{14} - \mathrm{D}_3}{\delta_3 N_{\mathrm{Old\_B}}}\right)\right)^2 + 4\frac{J_{14} - \mathrm{D}_4}{\delta_4}}\right] \\ N_{\mathrm{Osteoid}} &= 1/2\left[-\left(\beta_{13} - \beta_{10} + \frac{J_{14} - \mathrm{D}_4}{\delta_4 N_{\mathrm{Activ\_OB}}}\right) + \sqrt{\left(\beta_{13} - \beta_{10} + \frac{J_{14} - \mathrm{D}_4}{\delta_4 N_{\mathrm{Activ\_OB}}}\right)^2 + 4\frac{J_{14} - \mathrm{D}_5}{\delta_5}}\right] \\ N_{\mathrm{New\_B}} &= -N_{\mathrm{Osteoid}} - \beta_{10} - \frac{J_{14} - \mathrm{D}_4}{\delta_4 N_{\mathrm{Activ\_OB}}} \end{aligned} \tag{C1}$$

where N_i is the positive normalized concentration in stationary solution.

APPENDIX D

Conditions for Osanger coefficients

By substituting Eqs. (9) and (10) into Eq. (8), the following quadratic equation is obtained,

$$\left(l_{\mathrm{vv}} d_{(1)} + l_{\mathrm{v}\rho} A_\rho\right) d_{(1)} + \left(l_{\rho\mathrm{v}} d_{(1)} + l_{\rho\rho} A_\rho\right) A_\rho \geq 0$$

As $l_{\mathrm{v}\rho} = l_{\rho\mathrm{v}}$ (Osanger's reciprocal relation), the aforementioned equation can be amended as follows

$$l_{\mathrm{vv}}\left(\frac{d_{(1)}}{A_\rho}\right)^2 + 2l_{\rho\mathrm{v}}\left(\frac{d_{(1)}}{A_\rho}\right) + l_{\rho\rho} \geq 0$$

This in equation is satisfied only if

$$\begin{cases} l_{\mathrm{vv}} > 0 \ \ \& \ \ l_{\rho\rho} > 0 \ \ \text{and} \\ -1 < q = \frac{l_{\mathrm{v}\rho}}{\sqrt{l_{\mathrm{vv}} l_{\rho\rho}}} < 1 \end{cases} \tag{D1}$$

References

1. Buford A, Goswami T. Review of wear mechanisms in hip implants: Paper I—General. Mater Des 2004;25:385–393.
2. Cristofolini L. A critical analysis of stress shielding evaluation of hip prostheses. Crit Rev Biomed Eng 1997;25:409–483.
3. Huiskes R, Weinans H, Rietbergen BV. The relationship between stress shielding and bone resorption around total hip stems and effects of flexible materials. Clin Orthop Relat Res 1992;274:124–134.
4. Weinans H, Huiskes R, Grootenboer HJ. The behavior of adaptive bone-remodeling simulation models. J Biomech 1992;25:1425–1441.
5. Taylor M, Verdonschot N, Huiskes R, Zioupos P. A combined finite element method and continuum damage mechan-

ics approach to simulate the in vitro fatigue behavior of human cortical bone. J Mater Sci: Mater Med 1999;10:841–846.
6. Mullender M, Huiskes R. Proposal for the regulatory mechanism of Wolff's law. J Orthop Res 1995;13:503–512.
7. Huiskes R, Weinans H, Grootenboer HJ, Dalstra M, Fudala B, Slooff TJ. Adaptive bone-remodeling theory applied to prosthetic-design analysis. J Biomech 1987;20:1135–1150.
8. Levenston M, Carter DR. An energy dissipation-based model for damage stimulated bone adaptation. J Biomech 1998;31: 579–586.
9. Hernandez C, Beaupré GS, Carter DR. A model of mechanobiologic and metabolic influences on bone adaptation. J Rehabil ResDev 2000;37:235–244.
10. Carter D, Beaupré GS. Skeletal Function and Form: Mechanobiology of Skeletal Development, Aging, and Regeneration. Cambridge, UK: Cambridge University Press; 2001.
11. Rouhi G, Epstein M, Sudak L, Herzog W. Modeling bone resorption using mixture theory with chemical reactions. J Mech Mater Struct 2007;2:1141–1155.
12. Lemaire V, Tobin FL, Greller LD, Cho CR, Suva LJ. Modeling the interactions between osteoblast and osteoclast activities in bone remodeling. J Theor Biol 2004;229:293–309.
13. Huiskes R, Ruimerman R, van Lenthe GH, Janssen JD. Effects of mechanical forces on maintenance and adaptation of form in trabecular bone. Nature 2000;405:704–706.
14. Prendergast PJ, Taylor D. Prediction of bone adaptation using damage accumulation. J Biomech 1994;27:1067–1076.
15. Levenston ME, Carter DR. An energy dissipation-based model for damage stimulated bone adaptation. J Biomech 1998;31:579–586.
16. Frost HM. Changing concepts in skeletal physiology: Wolff's law, the mechanostat, and the "Utah Paradigm". Am J Hum Biol 1998;10:599–605.
17. Hernandez CJ, Beaupre GS, Carter DR. A model of mechanobiologic and metabolic influences on bone adaptation. J Rehabil Res Dev 2000;37:235–244.
18. Ruimerman R, Huiskes R, Van Lenthe GH, Janssen JD. A computer-simulation model relating bone-cell metabolism, to mechanical adaptation of trabecular bone. Comput Meth Biomed Bioeng 2001;4:433–448.
19. Kroll MH. Parathyroid hormone temporal effects on bone formation and resorption. Bull Math Biol 2000;62:163–188.
20. Rattanakul C, Lenbury Y, Krishnamara N, Wollkind DJ. Modeling of bone formation and resorption mediated by parathyroid hormone: Response to estrogen/PTH therapy. BioSystems 2003;70:55–72.
21. Komarova SV, Smith RJ, Dixon SJ, Sims SM, Wahl LM. Mathematical model predicts a critical role for osteoclast autocrine regulation in the control of bone remodeling. Bone 2003;33:206–215.
22. Ehrlich PJ, Lanyon LE. Mechanical strain and bone cell function: A review. Osteoporos Int 2002;13:688–700.
23. Klika V, Maršík F. Bone remodeling driven by dynamic loading and drug treatment. Presented at Human Biomechanics Conference, Prague, Czech Republic, 2008.
24. Bougherara H, Bureau MN, Yahia L. Bone remodeling in a new biomimetic polymer-composite hip stem. Journal of Biomedical Materials Research A 2010;92:164–174.
25. Petrtýl M, Danešová J. Principles of bone remodelling—The limit cycles of bone remodelling. Acta Bioeng Biomech 2001; 3:75–91.
26. Bejan A, Marden JH. Unifying constructal theory for scale effects in running, swimming and flying. J Exp Biol 2006; 209:238–248.
27. Michaelis L, Menten ML. Kinetik der Invertinwirkung. Biochem Z 1913;49:333–369.
28. Ignetik R, Deakin MAB. Asymptotic analysis of the Michaelis-Menten reaction equations. Bull Math Biol 1981;43:375–388.
29. Nicolis G, Prigogine I. Selforganization in Nonequilibrium Systems. New York: Wiley; 1977.
30. Öttinger HC. Beyond Equilibrium Thermodynamics. Hoboken, New Jersy: John Wiley; 2005. p 656.
31. Cowin SC, Weinbaum S, Zeng Y. A case for bone canaliculi as the anatomical site of strain generated potentials. J Biomech 1995;28:1281–1297.
32. Onsager L. Reciprocal relations in irreversible processes I. Phys Rev 1931;37:405–426.
33. Onsager L. Reciprocal relations in irreversible processes II. Phys Rev 1931;38:2265–2279.
34. Jagers P, Klebaner F. Random variation and concentration effects in PCR. J Theor Biol 2003;224:299–304.
35. Bejan A. Shape and Structure from Engineering to Nature. Cambridge: Cambridge University Press; 2000.
36. Cohen ER, Cvitaš T, Frey JG, Holmström B, Kuchitsu K, Marquardt R, Mills I, Pavese F, Quack M, Stohner J, Strauss HL, Takami M, Thor AJ. Quantities, Units and Symbols in Physical, 3rd ed. Cambridge: The Royal Society of Chemistry; 2007.
37. Muller P. Glossary of terms used in physical organic chemistry Pure Appl Chem 1994;66:1077–1184.
38. Heineken F, Tsuchiya HM, Aris R. On the mathematical status of the pseudo-steady state hypothesis of biochemical kinetics. Math Biosci 1967;1:95–113.
39. Klika V. Matematická analýza a numerická simulace remodelačních procesův kostech [Translation: Mathematical and numerical analysis of differential equations of bone remodeling]. M.Sc. Thesis, Prague, Czech Republic, CTU Prague, 2006.
40. Abe H, Hayashi K, Sato M. Data Book on Mechanical Properties of Living Cells, Tissues, and Organs. New York: Springer; 1996. p 436.
41. Kuhl E, Balle F. Computaional modeling of hip replacement surgery: Total hip replacement vs. hip resurfacing. Technische Mecanik 2005;25:107–114.
42. Sadd MH. Elasticity: Theory, Applications and Numerics. Burlington: Elsevier Academic Press; 2005.
43. Daniel I, Ishai O. Engineering Mechanics of Composite Materials, 2nd ed. New York: Oxford University Press; 2005.
44. Carter DR, Orr TE, Fyhrie DP. Relationships between loading history and femoral cancellous bone architecture. J Biomech 1989;22:231–244.
45. Lotz JC, Gerhart TN, Hayes WC. Mechanical properties of metaphyseal bone in the proximal femur. J Biomech 1991; 24:317–329.
46. Goulet RW, Goldstein SA, Ciarelli MJ, Kuhn JL, Brown MB, Feldkamp LA. The relationship between the structural and orthogonal compressive properties of trabecular bone. J Biomech 1994;27:375–389.
47. Kopperdahl DL, Keaveny TM. Yield strain behavior of trabecular bone. J Biomech 1998;31:601–608.
48. Ciarelli TE, Fyhrie DP, Schaffler MB, Goldstein SA. Variations in three-dimensional cancellous bone architecture of the proximal femur in female hip fractures and in controls. J Bone Miner Res 2000;15:32–40.
49. Helgason B, Perilli E, Schileo E, Taddei F, Brynjólfsson S, Viceconti M. Mathematical relationships between bone density and mechanical properties: A literature review. Clin Biomech 2008;23:135–146.
50. Torcasio A, van Lenthe GH, Van Oosterwyck H. The importance of loading frequency, rate and vibration for enhancing bone adaptation and implant osseointegration. Eur Cells Mater 2008;16:56–68.
51. Rubin C, Lanyon L. Regulation of bone mass by mechanical strain magnitude. Calcif Tissue Int 1985;37:411–417.
52. Truong L-H, Kuliwaba J, Tsangari H, Fazzalari N. Differential gene expression of bone anabolic factors and trabecular bone architectural changes in the proximal femoral shaft of pri-

mary hip osteoarthritis patients. Arthritis Res Ther 2006;8: R188.
53. Ehrlich P, Lanyon LE. Mechanical strain and bone cell function: A review. Osteop Int 2002;13:688–700.
54. Jaworski ZFG, Uhthoff HK. Reversibility of nontraumatic disuse osteoporosis during its active phase. Bone 1986;7:431–439.
55. Nagel A, Fernholz F, Kibele C, Rosenbaum D. Long distance running increases plantar pressures beneath the metatarsal heads: A barefoot walking investigation of 200 marathon runners. Gait Posture 2008;27:152–155.
56. Theis J, Ball C. Medium-term results of cementless hydroxyapatite-coated primary total hip arthroplasty: A clinical and radiological review. J Orthop Surg (Hong Kong) 2003;11:159–165.
57. Gupta S, New AMR, Taylor M. Bone remodelling inside a cemented resurfaced femoral head. Clin Biomech 2006;21: 594–602.
58. Schiltz C, Marty C, De Vernejoul MC, Geoffroy V. Inhibition of osteoblastic metalloproteinases in mice prevents bone loss induced by oestrogen deficiency. J Cell Biochem 2008;104: 1803–1817.
59. Judex S, Zernicke RF. High-impact exercise and growing bone: Relation between high strain rates and enhanced bone formation. J Appl Physiol 2000;88:2183–2191.
60. Adami S, Gatti D, Viapiana O, Fiore CE, Nuti R, Luisetto G, Ponte M, Rossini M; BONTURNO Study Group. Physical activity and bone turnover markers: A cross-sectional and a longitudinal study. Calcif Tissue Int 2008;83:388–392.
61. Carter DR. Mechanical loading histories and cortical bone remodeling. Calcif Tissue Int 1984;36(Suppl 1):S19–S24.
62. Van Rietbergen B, Huiskes R, Eckstein F, Ruegsegger P. Trabecular bone tissue strains in the healthy and osteoporotic human femur. J Bone Miner Res 2003;18:1781–1788.
63. Gilsanz V, Wren TAL, Sanchez M, Dorey F, Judex S, Rubin C. Low-level. High-frequency mechanical signals enhance musculoskeletal development of young women with low BMD. J Bone Miner Res 2006;21:1464–1474.
64. Passeri G, Vescovini R, Sansoni P, Galli C, Franceschi C, Passeri M. Calcium metabolism and vitamin D in the extreme longevity. Exp Gerontol 2008;43:79–87.
65. Viljakainen HT, Väisänen M, Kemi V, Rikkonen T, Kröger H, Laitinen EK, Rita H, Lamberg-Allardt C. Wintertime vitamin D supplementation inhibits seasonal variation of calcitropic hormones and maintains bone turnover in healthy men. J Bone Miner Res 2009;24:346–352.
66. Kitazawa R, Imai Y, Fukase M, Fujita T. Effects of continuous infusion of parathyroid hormone and parathyroid hormone-related peptide on rat bone in vivo: comparative study by histomorphometry. Bone Miner 1991;12:157–166.
67. Watson PH, Fraher LJ, Kisiel M, Desousa D, Hendy G, Hodsman AB. Enhanced osteoblast development after continuous infusion of hPTH(1–84) in the rat. Bone 1999;24:89–94.
68. Parfitt AM. The actions of parathyroid hormone on bone: Relation to bone remodeling and turnover, calcium homeostasis, and metabolic bone diseases: Part II of IV parts: PTH and bone cells: Bone turnover and plasma calcium regulation. Metabolism 1976;25:909–955.
69. Du P, Ye Y, Seitz PK, Bi LG, Li H, Wang C, Simmons DJ, Cooper CW. Endogenous parathyroid hormone-related peptide enhances proliferation and inhibits differentiation in the osteoblast-like cell line ROS 17/2.8. Bone 2000;26:429–436.
70. Huiskes R, Boeklagen R. Mathematical shape optimization of hip prosthesis design. J Biomech 1989;22:793–804.
71. Weinans H, Huiskes R, Grootenboer HJ. The behavior of adaptive bone-remodeling simulation models. J Biomech 1992;25:1425–1441.
72. Cowin S, Hegedus DH. Bone remodeling I: Theory of adaptive elasticity. J Elasticity 1976;6:313–326.
73. Bland R. Steroid hormone receptor expression and action in bone. Clin Sci (Lond) 2000;98:217–240.
74. Schmidt SM, McCready MJ, Ostafin AE. Effect of oscillating fluid shear on solute transport in cortical bone. J Biomech 2005;38:2337–2343.
75. Glansdorff P, Prigogine I. Thermodynamics Theory of Structure, Stability and Fluctuations. London: Wiley-Interscience; 1971.